




Ruthenium dinitrosyl complexes – computational characterization of structure and reactivity

Amr A.A. Attia, Ilia A. Dereven'kov & Radu Silaghi-Dumitrescu

To cite this article: Amr A.A. Attia, Ilia A. Dereven'kov & Radu Silaghi-Dumitrescu (2015) Ruthenium dinitrosyl complexes – computational characterization of structure and reactivity, Journal of Coordination Chemistry, 68:14, 2409-2422, DOI: [10.1080/00958972.2015.1041936](https://doi.org/10.1080/00958972.2015.1041936)


To link to this article: <http://dx.doi.org/10.1080/00958972.2015.1041936>

 View supplementary material 

 Accepted author version posted online: 18 Apr 2015.
Published online: 11 May 2015.

 Submit your article to this journal 

 Article views: 84

 View related articles 

 View Crossmark data 

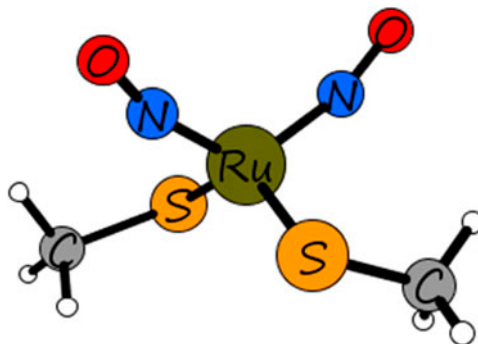
Ruthenium dinitrosyl complexes – computational characterization of structure and reactivity

AMR A.A. ATTIA[†], ILIA A. DEREVEN'KOV[‡] and RADU SILAGHI-DUMITRESCU^{*†}

[†]Department of Chemistry, Babes-Bolyai University, Cluj-Napoca, Romania

[‡]Department of Food Chemistry and Biotechnology, Ivanovo State University of Chemistry and Technology, Ivanovo, Russia

(Received 18 December 2014; accepted 26 March 2015)



Elucidation of the electronic structure of a dinitrosyl dithiolate ruthenium complex in several formal oxidation states ranging from Ru(I) to Ru(III) has been undertaken. DFT and *ab initio* molecular dynamics simulations have shown clear evidence of asymmetry within the dinitrosyl moieties in all models though most noticeably in the excited states. The reaction pathway of a hyponitrite adduct formation was also examined and found to be more feasible in the excited states. These results, along with the recently reported study on the dinitrosyl dithiolate iron analog of these complexes, provide insight toward the mechanism of NO donation by dinitrosyl metal complexes.

Keywords: DFT; Dinitrosyl; Ruthenium; Nitric oxide; Thiolate; DNIC

1. Introduction

Due to the important role that NO plays in various biological processes [1–12], a considerable amount of research has been generated on NO donation activities of various nitrosyl metal complexes with nitrosyl iron complexes holding the biggest share [13–26]. The ability of dinitrosyl iron complexes with thiol containing ligands to act as NO donors as well

*Corresponding author. Email: rsilaghi@chem.ubbcluj.ro

as their strong pharmacological potential has been reviewed [27]. Ruthenium-based nitrosyl complexes have gained attention recently, as they were also found to be promising NO carriers [28–54]; a recent detailed account on the biological activities of ruthenium nitrosyl complexes is available [55].

Ruthenium dinitrosyl complexes received less attention than mononitrosyl ones. Among the reported complexes are the synthesized and structurally characterized $\{\text{Ru}(\text{NO})_2\}^{10}$ (by Enemark and Feltham notation; formally Ru(0)) four-coordinate complexes containing two triphenylphosphine ligands [56, 57] and the $\{\text{Ru}(\text{NO})_2\}^8$ (formally Ru(II)) five-coordinate complexes containing two triphenylphosphines (or other phosphines) and one chloride [58–60]. It was believed earlier that, in the latter case, NO moieties only occupy linear and bent orientations as indicated by X-ray crystallography [59, 60], implying the existence of NO^+ and $^1\text{NO}^-$ ligands dynamically interconverting [60]. However, recent studies have revealed the existence of additional isomers exhibiting more symmetric structures [58]. Additionally, a dinitrosyl Ru adduct was detected in the pathway of $[\text{Ru}(\text{porphyrin})(\text{NO})(\text{NO}_2)]$ as reported by Ford and coworkers [61]. While there is no experimental evidence suggesting the dimerization of NO ligands within Ru dinitrosyls [57] giving hyponitrite adducts, these adducts were observed in binuclear Ru nitrosyls with NO moieties attached to neighboring metal centers [62]. Hence, this point needs further clarification.

We recently reported a theoretical investigation on a dinitrosyl dithiolate iron complex with iron oxidation states ranging from Fe(0) to Fe(III). Results obtained from DFT, MC-CASSCF as well as *ab initio* molecular dynamics (AIMD) simulations revealed stark asymmetry between the NO ligands within each complex in all oxidation states [63]. Likewise, asymmetrical behavior of the dinitrosyl moieties was also noticeable in reaction pathways leading to formation of hyponitrite adduct. We concluded that this asymmetry could hold the key to the mechanism of NO donation by DNICs [63].

Thus, elucidation of the electronic structure as well as the isomerism within dinitrosyl ruthenium complexes is essential. No attempts have been made to solve the electronic structure of dinitrosyl ruthenium complexes with thiol containing ligands. In this study, we follow the same strategy of our previous report on DNICs: we carry out a theoretical investigation on a dithiolate dinitrosyl ruthenium complex, depicted in figure 1, by employing DFT and AIMD simulations on several formal oxidation states of ruthenium ranging from Ru(I) to Ru(III) and, in addition, we explore the reaction pathways leading to the formation of a hyponitrite moiety within each complex; along our line of discussion we compare the results obtained in this report with our previous work on iron analogs of these models [63]. The results obtained provide insight toward the mechanism of NO donation by dinitrosyl ruthenium complexes.

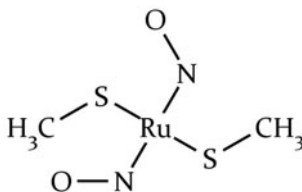


Figure 1. Schematic representation of the dinitrosyl dithiolate ruthenium complex investigated in this study.

2. Models and theoretical methods

The structure investigated in this study is a mononuclear dinitrosyl dithiolate ruthenium complex. Ru(I), Ru(II), and Ru(III) oxidation states were taken into consideration, thus three models, $[\text{Ru}(\text{SCH}_3)_2(\text{NO})_2]^-$, $[\text{Ru}(\text{SCH}_3)_2(\text{NO})_2]^0$, and $[\text{Ru}(\text{SCH}_3)_2(\text{NO})_2]^+$ were investigated. The total charge of each model was adjusted taking into account the anionic character of thiolate, the neutral nitric oxide, and the proper charge of ruthenium corresponding to its oxidation state.

Structure optimizations at the DFT level of theory were performed using the Gaussian 09 software package [64] with GaussView [65] as front end. The meta GGA DFT functional M06-L [66] was utilized in all calculations. We point out that the M06-L functional has been designed to include medium-range electron correlation effects (dispersion effects), and has been specifically recommended for transition metal containing systems; M06-L offered the best agreement of several tested functionals compared to large multireference calculations, and several benchmark studies have confirmed its excellent accuracy [67–73]. The SDD (Stuttgart/Dresden effective core potential) basis set [74] was applied for ruthenium, while the triple zeta 6-311+G(d,p) basis set was employed for the rest of the atoms. Unless otherwise stated, all optimizations were carried out using the unrestricted formalism, wave function stability tests were carried out to confirm the energetic minimum, and vibrational analyses were performed for each structure to ensure the absence of imaginary frequencies. Computed geometric parameters, Mulliken atomic spin densities, Mulliken atomic charges, and relative energies for all models were summarized. Hirshfeld population is also reported and can be viewed in the supporting information. Solvation calculations in water were performed by employing the Conductor-like Polarizable Continuum Model [75] as implemented in Gaussian 09. Potential energy surfaces (PES) of N–N bond formation were calculated for the ground state and excited state of each model using the coordinate driving functions within the Gaussian 09 software package. The N–N bond length was systematically decreased by 0.2 Å and the structure was optimized with a fixed N–N bond length after each step down to an N–N interatomic distance of 1.45 Å. AIMD simulations were performed using the extended Lagrangian approach with the atom centered density matrix propagation model [76] utilizing the same DFT functional and basis sets. AIMD calculations were run at room temperature, with converged SCF result at each point and a time step of 1 fs. Structure visualizations were performed using the XYZviewer visualization program [77].

3. Results and discussion

3.1. Ground states versus excited states in dinitrosyl ruthenium models

Optimized structures of all ruthenium models have shown a preference for the tetrahedral structural conformation with distortions most noticeable in the high-spin states – results that are in agreement with those obtained from the iron analogs of these complexes [63].

As illustrated in tables 1 and 2 and depicted in figure 2, the neutral model, i.e. $[\text{Ru}(\text{SCH}_3)_2(\text{NO})_2]^0$ with the formal Ru(II) oxidation state features a low spin $S = 0$ ground state with symmetry with respect to the two NO ligands – identical N–O, Ru–N, and Ru–S bond lengths as well as Ru–N–O bond angles, similar partial atomic charges and spin

Table 1. Relative energies (kcal mol^{-1}), bond lengths (\AA), bond angles (degrees), and population analyses for $[\text{Ru}(\text{SCH}_3)_2(\text{NO})_2]^0$, as obtained from (UM06-L/SDD on Ru, 6-311+G(d,p) on rest of the atoms) calculations.

<i>S</i>	ΔE	Ru-N			N-O			Ru-S			Ru-N-O			Atomic spin densities			Atomic charges		
		Ru-N	N-O	Ru-S	Ru-S	Ru-N-O	Ru	(NO) ₂	(SCH ₃) ₂	Ru	(NO) ₂	(SCH ₃) ₂	Ru	(NO) ₂	(SCH ₃) ₂				
0	0.0	1.78//1.78	1.16//1.16	2.31//2.31	163//163	0.00	0.00//0.00	0.00	1.04	-0.25// -0.25	0.00	1.04	-0.25// -0.25	-0.52					
1	18.4	1.83//1.83	1.16//1.16	2.30//2.30	170//170	0.44	0.40//0.40	0.70	1.39	-0.68// -0.69	0.70	1.39	-0.68// -0.69	-0.02					
2	44.1	1.85//1.98	1.18//1.18	2.28//2.29	144//152	1.38	0.56//1.28	0.81	0.66	-0.21// -0.22	0.81	0.66	-0.21// -0.22	-0.10					

Table 2. Relative energies, bond lengths, bond angles, and population analyses for $[\text{Ru}(\text{SCH}_3)_2(\text{NO})_2]^0$, as obtained from (UM06-L/SDD on Ru, 6-311+G(d,p) on rest of the atoms) calculations in water.

<i>S</i>	ΔE	Ru–N	N–O	Ru–S	Ru–N–O	Atomic spin densities			Atomic charges		
						Ru	(NO) ₂	(SCH ₃) ₂	Ru	(NO) ₂	(SCH ₃) ₂
0	0.0	1.77//1.77	1.16//1.16	2.33//2.33	160//160	0.00	0.00//0.00	0.00	1.39	–0.31//–0.32	–0.81
1	16.7	1.81//1.82	1.16//1.16	2.31//2.31	164//165	0.32	0.48//0.52	0.68	1.24	–0.51//–0.47	–0.26
2	42.9	1.85//1.98	1.18//1.18	2.28//2.29	141//149	1.29	0.61//1.37	0.73	1.04	–0.23//–0.49	–0.31

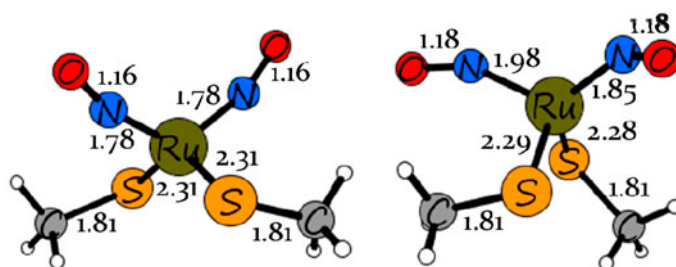


Figure 2. Optimized structures of the $[\text{Ru}(\text{SCH}_3)_2(\text{NO})_2]^0$ model in the $S = 0$ (left) and $S = 2$ (right) spin states.

densities. This is also consistent in the solvated model as shown in table 2. In the $S = 2$ excited state, an asymmetry in the Ru–N bond lengths in addition to Ru–N–O bond angles is clearly visible; a difference of 0.13 Å between Ru–N bond lengths and 8° between Ru–N–O bond angles is evident in vacuum and in solvent. However, N–O and Ru–S bond lengths as well as partial atomic charges are in perfect symmetry. Additionally, the distribution of spin densities shows twice as much spin on the elongated Ru–NO: a value of 1.3 spin units compared to 0.56 on the other NO. The uneven distribution of spin densities over the dinitrosyl moieties in the excited state *versus* the ground state is also clearly observed in figure 3; while in the $S = 0$ spin state the molecular orbitals relevant to the Ru–NO interaction are symmetrically delocalized over both NO ligands, in the $S = 2$ state the molecular orbitals are asymmetric (each delocalized predominantly over a single NO).

These results are consistent with those found for the ferrous analog of this model as reported in our previous study [63]. However, the asymmetric behavior is weaker in the ruthenium case; moreover, the excited state sits on a lower energy level ($\sim 17 \text{ kcal mol}^{-1}$) in the case of the iron model compared to $\sim 44 \text{ kcal mol}^{-1}$ in the ruthenium model. Weak influence of solvation on the relative energies and the geometrical parameters of the ruthenium model are observed – a result that is in contrast to the ferrous analog of the same complex [63]. In addition, the antiferromagnetic coupling between Fe and NO observed in the ferrous model is not noticeable in the ruthenium case [63].

This asymmetry, although only noticeable in the excited state which is $\sim 44 \text{ kcal mol}^{-1}$ higher in energy than the ground state, not only could hold the key to the mechanism by which dinitrosyl ruthenium complexes donate NO, but also could be relevant to the formation

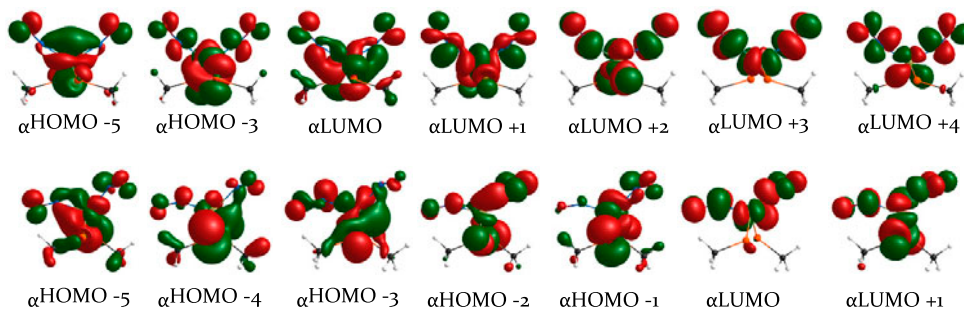


Figure 3. Illustrative frontier molecular orbitals for $[\text{Ru}(\text{SCH}_3)_2(\text{NO})_2]^0$. $S = 0$ (upper row) and $S = 2$ (lower row).

of a hyponitrite adduct as in the case of the nitric oxide scavenging enzyme nitric oxide reductase.

Results obtained from $[\text{Ru}(\text{SCH}_3)_2(\text{NO})_2]^{-1}$ and $[\text{Ru}(\text{SCH}_3)_2(\text{NO})_2]^{+1}$ as shown in tables 3 and 4, respectively, were in line with $[\text{Ru}(\text{SCH}_3)_2(\text{NO})_2]^0$ concerning the ground state preference as well as the asymmetry noticed for Ru–NO bond lengths and Ru–N–O bond angles in the excited states. Molecular orbital diagrams reinforce this asymmetry as well and can be viewed in the supporting information. This is also consistent with the iron analogs of these models as reported previously [63].

3.2. AIMD simulations

AIMD simulations performed on all oxidation states for 500 fs provided additional evidence for asymmetry between the nitrosyl ligands. In the ground state of the neutral model, i.e. the formally Ru(II) structure, Ru–N bonds propagate in a fixed range of 0.25 Å, but do so in an asymmetric manner, while N–O bond trajectories show perfect symmetry until the end of the simulation. The excited state case was not different, the trajectories showed a clear case of asymmetry between the nitrosyl ligands: both Ru–N bonds are propagating in a 0.4 Å range with clear asymmetry. N–O bond propagations, however, exhibited perfect symmetries for both nitrosyl adducts in the excited state as well as in the ground state.

Trajectories obtained from the Ru(I) model agree with the Ru(II) case in showing an interesting case of asymmetry for the Ru–N bond propagation. Moreover, in the case of Ru(III) the asymmetry between both nitrosyl adducts was remarkably strong in the excited state: one adduct with Ru–N bond propagating asymmetrically in a 0.5 Å range, while the other Ru–N bond dissociates to reach a distance of 3.30 Å at the end of the simulation. N–O bond trajectories for the Ru(I) and Ru(III) were also conforming to those obtained from the Ru(II) model, i.e. exhibiting symmetrical propagations in a fixed distance range throughout the simulation. Graphical trajectories of all simulations can be viewed in the supporting information.

These results are in accordance with those previously reported on the iron analogs of these models; however, the asymmetry was more extreme in the iron case where NO dissociation was observable in the excited states of almost all models, and even in the ground states of some models [63]. This could be an indication of the stronger tendency of dinitrosyl iron complexes to donate NO compared to ruthenium complexes.

3.3. Reaction pathways leading to formation of nitrogen–nitrogen bonds

PES of N–N bond formation within the neutral dinitrosyl structure, formally Ru(II), in both the ground state and the excited state are depicted in figure 4. This hyponitrite adduct was found to cost ~ 44 kcal mol⁻¹ in the ground state and not associated with an energy minimum at any point along the profile, whereas in the excited state (i.e. $S = 2$) the profile starts out exergonically for the first 0.2 Å then increases to ~ 38 kcal mol⁻¹ until a full N–N bond is formed; this is coupled with an energy minimum at the middle of the reaction pathway. The formation of a hyponitrite adduct is then found to cost almost the same energy in both the ground state and the excited state for the Ru(II) model despite the clear asymmetry in Ru–N bond lengths in the excited state. For comparison, the N–N bond formation reported for the ferrous analog of this complex was much more feasible in the excited state [63].

Table 3. Relative energies, bond lengths, bond angles, and population analyses for $[\text{Ru}(\text{SCH}_3)_2(\text{NO})_2]^{-1}$, as obtained from (UM06-L/SDD on Ru, 6-311+G(d,p) on rest of the atoms) calculations.

<i>S</i>	ΔE	Ru-N	N-O	Ru-S	Ru-N-O	Atomic spin densities			Atomic charges		
						Ru	(NO) ₂	(SCH ₃) ₂	Ru	(NO) ₂	(SCH ₃) ₂
1/2	0.0	1.78//1.78	1.19//1.19	2.42//2.42	166//168	0.83	-0.10// -0.10	0.39	0.62	-0.46// -0.46	-0.38
3/2	23.9	1.80//1.92	1.18//1.19	2.38//2.41	155//165	0.33	0.79//1.31	0.48	0.42	-0.30// -0.05	-1.10
5/2	53.4	1.88//2.09	1.20//1.21	2.38//2.38	146//135	2.12	0.75//1.42	0.56	0.85	-0.31// -0.43	-0.23

Table 4. Relative energies, bond lengths, bond angles, and population analyses for $[\text{Ru}(\text{SCH}_3)_2(\text{NO})_2]^+$, as obtained from (UM06-L/SDD on Ru, 6-311+G(d,p) on rest of the atoms) calculations.

<i>S</i>	ΔE	Ru–N	N–O	Ru–S	Ru–N–O	Atomic spin densities			Atomic charges		
						Ru	(NO) ₂	(SCH ₃) ₂	Ru	(NO) ₂	(SCH ₃) ₂
1/2	0.0	1.81//1.81	1.14//1.14	2.26//2.26	167//167	–0.06	0.22//0.22	0.38	0.94	–0.05//–0.05	0.31
3/2	42.7	1.78//2.03	1.14//1.14	2.32//2.30	177//178	0.84	0.23//0.91	0.99	1.32	–0.42//–0.15	–0.43
5/2	54.8	1.95//1.99	1.16//1.15	2.25//2.29	141//148	1.61	1.04//0.86	1.41	0.56	0.02//0.07	0.31

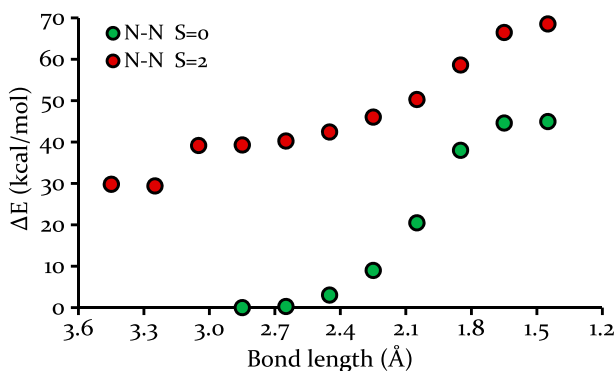


Figure 4. N–N bond formations in the ground states and excited states of Ru(II) dinitrosyl dithiolate structure. Low spin energy was considered as an arbitrary reference.

N–N bonding was slightly different in the case of the positively charged structure, i.e. formally Ru(III): the graphical presentation shown in figure 5 illustrates that the energy barrier for an N–N bond formation was much higher in the ground state with a linear pattern requiring ~ 80 kcal mol⁻¹. However, no local minimum was formed at the end of the energy profile as observed for the neutral structure. N–N bond formation in the excited state, on the other hand, required half as much energy as in the ground state with an energy barrier of ~ 43 kcal mol⁻¹. A linear reaction profile was also the case in the excited state with a local maximum at 2.4 Å.

An exploration of the PES along the N–N bond for the formally Ru(I) structure revealed a different pattern when compared with its Ru(III) and Ru(II) counterparts. Figure 6 shows that the energy cost for the N–N bond formation was ~ 53 kcal mol⁻¹ in the ground state with a local maximum near the end of the profile; however, in the excited state the energy barrier was relatively low being at ~ 17 kcal mol⁻¹ for N–N bond formation.

All oxidation states, aside from the Ru(II), clearly favored the excited state for forming an N–N bond; only in the Ru(III) case was the energy barrier reasonable, at ~ 17 kcal mol⁻¹ – though being 58 kcal mol⁻¹ higher in energy than the ground state. Conversely, the

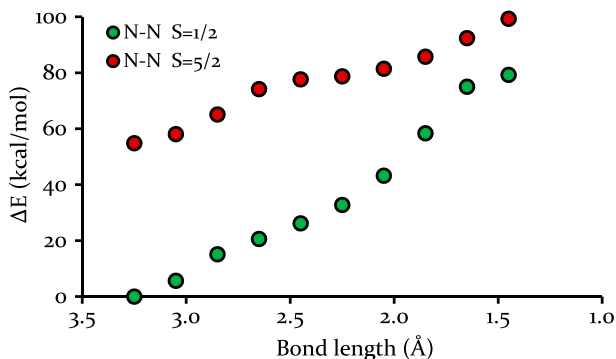


Figure 5. N–N bond formations in the ground states and excited states of Ru(III) dinitrosyl dithiolate structure. Low spin energy was considered as an arbitrary reference.

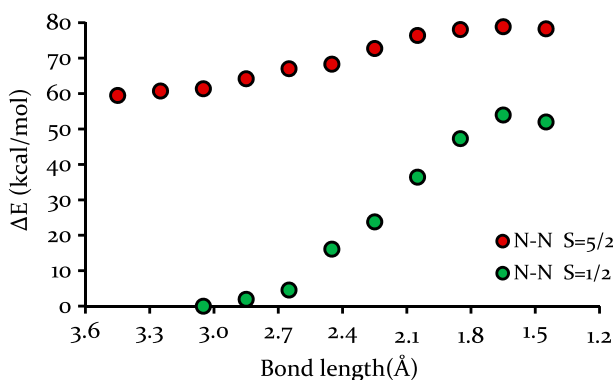


Figure 6. N–N bond formations in the ground states and excited states of Ru(I) dinitrosyl dithiolate structure. Low spin energy was considered as an arbitrary reference.

formation of such bond in the ground states of all models was extremely difficult, with the lowest barrier set at 44 kcal mol^{-1} in the Ru(II) case. This matches the results obtained for the iron analogs as reported in our previous study [63].

Table 5 illustrates the energies of the frontier orbitals for the low- and high-spin states of the Ru(II) model *versus* its ferrous analog. In the $S = 0$ ferrous case, HOMO–2 and HOMO–1 are nearly degenerate (0.03 eV difference), as are LUMO+1 and LUMO+2 (0.08 eV, with LUMO+3 remaining close in energy as well). An attempt to turn this ferrous system into $S = 1$ would lead to a hole in the old HOMO and to half-occupation of the old LUMO – none of which are in the degenerate sets; not surprisingly then, no distortion was seen in the $S = 1$ Fe(II) dinitrosyl system [63]. In contrast, the $S = 2$ ferrous state would involve half-occupation of the old HOMO and HOMO–1 as well as of the old LUMO and LUMO+1, bringing about two degeneracy problems: the HOMO–1 and HOMO–2 (now HOMO–3 and HOMO–4, respectively, on the α -manifold of the $S = 2$ state, with three electrons present in two orbitals previously of similar energy) *and* the LUMO+1 and LUMO+2 (now HOMO and LUMO, respectively, on the α -manifold of the $S = 2$ state, with one electron present in a pair of orbitals previously of similar energy). As a consequence, a severe distortion of the symmetry of the system occurs, with the two Fe–NO bonds $\sim 0.25 \text{ \AA}$ different from each other [63]. The α -HOMO–4/HOMO–3 gap is now 0.23 eV and the α -HOMO/LUMO gap is 0.90 eV.

Table 5. Energies (eV) of the frontier molecular orbitals of $[\text{Ru}(\text{SCH}_3)_2(\text{NO})_2]^0$ and its ferrous analog in the low- and high-spin states.

Molecular orbitals	$[\text{Fe}(\text{SCH}_3)_2(\text{NO})_2]^0$ $S = 0$	$[\text{Fe}(\text{SCH}_3)_2(\text{NO})_2]^0$ $S = 2 (\alpha)$	$[\text{Ru}(\text{SCH}_3)_2(\text{NO})_2]^0$ $S = 0$	$[\text{Ru}(\text{SCH}_3)_2(\text{NO})_2]^0$ $S = 2 (\alpha)$
HOMO–2	–6.40540	–6.06071	–6.40499	–5.50979
HOMO–1	–6.37171	–5.66457	–6.27623	–5.19398
HOMO	–5.35273	–5.01544	–5.36846	–4.81492
LUMO	–4.16119	–4.11055	–3.7478	–3.38507
LUMO+1	–3.26118	–3.41974	–3.08689	–3.23282
LUMO+2	–3.17587	–3.29623	–3.04643	–2.52141
LUMO+3	–3.09059	–0.31320	–2.85605	–0.35661

In the Ru(II) $S = 0$ case, a similar degeneracy is seen in the LUMO+1/LUMO+2 pair (0.04 eV energy difference), but less so in the HOMO–2/HOMO–1 pair (0.13 eV energy difference). In line with the observations above, the $S = 1$ Ru(II) system is essentially undistorted, while the $S = 2$ state is indeed distorted, but with the difference between the two metal–NO bonds now at ~half the difference seen in the $S = 2$ ferrous counterpart.

4. Conclusion

DFT data reveal evidence for an asymmetric behavior within ruthenium dithiolate dinitrosyl models in formal oxidation states ranging from Ru(I) to Ru(III). This asymmetry was more persistent in the excited states. This phenomenon revealed itself in molecular dynamics calculations as well as in reaction pathways connecting the dinitrosyl state to a putative hyponitrite adduct. These results were all in agreement with our previous report on the iron analogs of these models. The asymmetry within the dinitrosyl moieties could hold the key to explaining the mechanism of NO donation by dinitrosyl metal complexes.

Disclosure statement

No potential conflict of interest was reported by the authors.

Funding

This work was supported by Romanian Ministry of Education and Research [Grant PN-II-ID-PCE-2012-4-0488].

Supplemental data

Supplemental data for this article can be accessed here [<http://10.1080/00958972.2015.1041936>].

References

- [1] C. Nathan. *FASEB J.*, **6**, 3051 (1992).
- [2] E. Culotta, D.E. Koshland. *Science*, **258**, 1861 (1992).
- [3] Y. Noda, A. Mori, R. Liburdy, L.J. Packer. *J. Pineal Res.*, **27**, 159 (1999).
- [4] V. Rettori, N. Belova, W.L. Dees, C.L. Nyberg, M. Gimeno, S.M. McCann. *Proc. Nat. Acad. Sci. U.S.A.*, **90**, 10130 (1993).
- [5] B.J.R. Whittle. *Histochem. J.*, **27**, 727 (1995).
- [6] S. Moncada, R.M.J. Palmer, A. Higgs. *Pharmacol. Rev.*, **43**, 109 (1991).
- [7] L.J. Ignarro. *Nitric Oxide: Biology and Pathobiology*, Academic Press, San Diego, CA (2000).
- [8] V. Bauer, R. Sotnikova. *Gen. Physiol. Biophys.*, **29**, 319 (2010).
- [9] L.J. Ignarro, G.M. Buga, K.S. Wood, R.E. Byrns, G. Chaudhuri. *Proc. Nat. Acad. Sci. U.S.A.*, **84**, 9265 (1987).
- [10] R.F. Furchgott. *Angew. Chem. Int. Ed.*, **38**, 1870 (1999).
- [11] S.A. Waldman, F. Murad. *Pharmacol. Rev.*, **39**, 163 (1987).
- [12] D.A. Wink, H.B. Hines, R.Y.S. Cheng, C.H. Switzer, W. Flores-Santana, M.P. Vitek, L.A. Ridnour. *J. Leukocyte Biol.*, **89**, 873 (2011).
- [13] A.F. Vanin. *Nitric Oxide*, **21**, 1 (2009).
- [14] V.L. Lakomkin, A.F. Vanin, A.A. Timoshin, V.I. Kapel'ko, E.I. Chazov. *Nitric Oxide Biol. Chem.*, **16**, 413 (2007).

- [15] K.B. Shumaev, A.F. Vanin, V.L. Lakomkin, V.P. Mokh, L.I. Serebryakova, O.V. Tskitishvili, A.A. Timoshin, A.V. Maksimenko, O.I. Pisarenko, E.K. Ruuge, V.I. Kapel'ko, E.I. Chazov. *Cardiological Vestnik (Rus.)*, **2**, 31 (2007).
- [16] V.L. Lakomkin, A.A. Timoshin, T.R. Orlova, S.A. Gubkina, A.N. Storozhilova, T.E. Gvozdkik, A.B. Dobrovol'sky, E.K. Ruuge, A.F. Vanin, V.I. Kapel'ko, B.A. Lapin, E.I. Chazov. *Kardiologiya (Rus.)*, **49**, 53 (2009).
- [17] A.F. Vanin, V.P. Mokh, V.A. Serezhenkov, E.I. Chazov. *Nitric Oxide Biol. Chem.*, **16**, 322 (2007).
- [18] A. Mülsch, P. Mordvintcev, A.F. Vanin, R. Busse. *FEBS Lett.*, **294**, 252 (1991).
- [19] Y.P. Vedernikov, P.I. Mordvintcev, I.V. Malenkova, A.F. Vanin. *Eur. J. Pharmacol.*, **211**, 313 (1992).
- [20] A.A. Timoshin, V.L. Lakomkin, E.K. Ruuge, A.F. Vanin. *Biofizika*, **57**, 331 (2012).
- [21] E.I. Chazov, O.V. Rodnenkov, A.V. Zorin, V.L. Lakomkin, V.V. Gramovich, O.N. Vyborov, A.G. Dragnev, A.A. Timoshin, L.I. Buryachkovskaya, A.A. Abramov, V.P. Massenko, E.V. Arzamastsev, V.I. Kapelko, A.F. Vanin. *Nitric Oxide*, **26**, 148 (2012).
- [22] A.F. Vanin. *Biofizika*, **56**, 868 (2011).
- [23] S.M. Brothers, M.Y. Darensbourg, M.B. Hall. *Inorg. Chem.*, **50**, 8532 (2011).
- [24] S. Ye, F. Neese. *J. Am. Chem. Soc.*, **132**, 3646 (2010).
- [25] S.W. Yeh, C.W. Lin, Y.W. Li, I.J. Hsu, C.H. Chen, L.Y. Jang, J.F. Lee, W.F. Liaw. *Inorg. Chem.*, **51**, 4076 (2012).
- [26] T.T. Lu, S.H. Lai, Y.W. Li, I.J. Hsu, L.Y. Jang, J.F. Lee, I.C. Chen, W.F. Liaw. *Inorg. Chem.*, **50**, 5396 (2011).
- [27] A.F. Vanin, D.S. Burbaev. *J. Biophys.*, **2011**, Article ID 878236, 14 pages (2011).
- [28] Y.X. Wang, P. Legzdins, J.S. Poon, C.Y.J. Pang. *J. Cardiovasc. Pharmacol.*, **35**, 73 (2000).
- [29] S.P. Fricker. *Platinum Met. Rev.*, **39**, 150 (1995).
- [30] S.P. Fricker, E. Slade, N.A. Powell, O.J. Vaughan, G.R. Henderson, B.A. Murrer, I.L. Megson, S.K. Bisland, F.W. Flitney. *Br. J. Pharmacol.*, **122**, 1441 (1997).
- [31] N.A. Davies, M.T. Wilson, E. Slade, S.P. Fricker, B.A. Murrer, N.A. Powell, G.R. Henderson. *Chem. Commun.*, 47 (1997).
- [32] F.G. Marcondes, A.A. Ferro, A.S. Torsoni, M. Sumitani, M.J. Clarke, D.W. Franco, E. Tfouni, M.H. Krieger. *Life Sci.*, **70**, 2735 (2002).
- [33] D. Bonaventura, R.L. de Lima, J.A. Vercesi, R.S. da Silva, L.M. Bendhack. *Vasc. Pharmacol.*, **46**, 215 (2007).
- [34] I. Szundi, M.J. Rose, I. Sen, A.A. Eroy-Reveles, P.K. Mascharak, Ó. Einarsdóttir. *Photochem. Photobiol.*, **82**, 1377 (2006).
- [35] E. Tfouni, F.G. Doro, L.E. Figueiredo, J.C.M. Pereira, G. Metzke, D.W. Franco. *Curr. Med. Chem.*, **17**, 3643 (2010).
- [36] A.D. Ostrowski, S.J. Deakin, B. Azhar, T.W. Miller, N. Franco, M.M. Cherney, A.J. Lee, J.N. Burstyn, J.M. Fukuto, I.L. Megson, P.C. Ford. *J. Med. Chem.*, **53**, 715 (2010).
- [37] A.D. Ostrowski, P.C. Ford. *Dalton Trans.*, 10660 (2009).
- [38] A.D. Pereira, P.C. Ford, R.S. da Silva, L.M. Bendhack. *Nitric Oxide*, **24**, 192 (2011).
- [39] G.M. Halpenny, K.R. Gandhi, P.K. Mascharak. *ACS Med. Chem. Lett.*, **1**, 180 (2010).
- [40] G. Von Poelhsitz, A.L. Bogado, M.P. de Araujo, H.S. Selistre- De-Araujo, J. Ellena, E.E. Castellano, A.A. Batista. *Polyhedron*, **26**, 4707 (2007).
- [41] P.C. Ford, J. Bourassa, K. Miranda, B. Lee, I. Lorkovic, S. Boggs, S. Kudo, L. Laverman. *Coord. Chem. Rev.*, **171**, 185 (1998).
- [42] J.A. Olabe. *Dalton Trans.*, 3633 (2008).
- [43] S.Y. Shaban, R. van Eldik. *Eur. J. Inorg. Chem.*, **2010**, 554 (2010).
- [44] P.G. Wang, M. Xian, X.P. Tang, X.J. Wu, Z. Wen, T.W. Cai, A.J. Janczuk. *Chem. Rev.*, **102**, 1091 (2002).
- [45] J.A. McCleverty. *Chem. Rev.*, **104**, 403 (2004).
- [46] M.J. Rose, P.K. Mascharak. *Coord. Chem. Rev.*, **252**, 2093 (2008).
- [47] J.J.N. Silva, W.R. Pavanelli, J.C.M. Pereira, J.S. Silva, D.W. Franco. *Antimicrob. Agents Chemother.*, **53**, 4414 (2009).
- [48] P.M.M. Guedes, F.S. Oliveira, F.R.S. Gutierrez, G.K. da Silva, G.J. Rodrigues, L.M. Bendhack, D.W. Franco, M.A. Do Valle Matta, D.S. Zamboni, R.S. da Silva, J.S. Silva. *Br. J. Pharmacol.*, **160**, 270 (2010).
- [49] E. Tfouni, F.G. Doro, A.S. Gomes, R.S. Silva, G. Metzker, P.G.Z. Benini, D.W. Franco. *Coord. Chem. Rev.*, **254**, 355 (2010).
- [50] E. Tfouni, M. Krieger, B.R. McGarvey, D.W. Franco. *Coord. Chem. Rev.*, **236**, 57 (2003).
- [51] E. Tfouni, K.Q. Ferreira, F.G. Doro, R.S. Silva, Z.N. Rocha. *Coord. Chem. Rev.*, **249**, 405 (2005).
- [52] D.R. Lang, J.A. Davis, L.G.F. Lopes, A.A. Ferro, L.C.G. Vasconcellos, D.W. Franco, E. Tfouni, A. Wieraszko, M.J. Clarke. *Inorg. Chem.*, **39**, 2294 (2000).
- [53] F.D. Oliveira, K.Q. Ferreira, D. Bonaventura, L.M. Bendhack, A.C. Tedesco, S.D. Machado, E. Tfouni, R.S. Silva. *J. Inorg. Biochem.*, **101**, 313 (2007).
- [54] R.M. Carlos, A.A. Ferro, H.A.S. Silva, M.G. Gomes, S.S.S. Borges, P.C. Ford, E. Tfouni, D.W. Franco. *Inorg. Chim. Acta*, **357**, 1381 (2004).

- [55] E. Tfouni, D.R. Truzzi, A. Tavares, A.J. Gomes, L.E. Figueiredo, D.W. Franco. *Nitric Oxide*, **26**, 38 (2012).
- [56] A.P. Gaughan Jr, B.J. Corden, R. Eisenberg, J.A. Ibers. *Inorg. Chem.*, **13**, 786 (1974).
- [57] N. Arulsamy, D.S. Bohle, J.A. Imonigie, R.C. Moore. *Polyhedron*, **26**, 4737 (2007).
- [58] A.K.E. Gallien, D. Schaniel, T. Woike, P. Klüfers. *Dalton Trans.*, **43**, 13278 (2014).
- [59] C.G. Pierpont, D.G. Van Derveer, W. Durland, R. Eisenberg. *J. Am. Chem. Soc.*, **92**, 4760 (1970).
- [60] D. Michael, P. Mingos, D.J. Sherman, I.D. Williams. *Transition Met. Chem.*, **12**, 493 (1987).
- [61] J.C. Patterson, I.M. Lorković, P.C. Ford. *Inorg. Chem.*, **42**, 4902 (2003).
- [62] Y. Arikawa, A. Ikeda, N. Matsumoto, K. Umakoshi. *Dalton Trans.*, **42**, 11626 (2013).
- [63] A.A.A. Attia, S.V. Makarov, A.F. Vanin, R. Silaghi-Dumitrescu. *Inorg. Chim. Acta*, **418**, 42 (2014).
- [64] M.J. Frisch, G.W. Trucks, H.B. Schlegel, G.E. Scuseria, M.A. Robb, J.R. Cheeseman, G. Scalmani, V. Barone, B. Mennucci, G.A. Petersson, H. Nakatsuji, M. Caricato, X. Li, H.P. Hratchian, A.F. Izmaylov, J. Bloino, G. Zheng, J.L. Sonnenberg, M. Hada, M. Ehara, K. Toyota, R. Fukuda, J. Hasegawa, M. Ishida, T. Nakajima, Y. Honda, O. Kitao, H. Nakai, T. Vreven, J.A. Montgomery, J.E. Jr. Peralta, F. Ogliaro, M. Bearpark, J.J. Heyd, E. Brothers, K.N. Kudin, V.N. Staroverov, R. Kobayashi, J. Normand, K. Raghavachari, A. Rendell, J.C. Burant, S.S. Iyengar, J. Tomasi, M. Cossi, N. Rega, J.M. Millam, M. Klene, J.E. Knox, J.B. Cross, V. Bakken, C. Adamo, J. Jaramillo, R. Gomperts, R.E. Stratmann, O. Yazyev, A.J. Austin, R. Cammi, C. Pomelli, J.W. Ochterski, R.L. Martin, K. Morokuma, V.G. Zakrzewski, G.A. Voth, P. Salvador, J.J. Dannenberg, S. Dapprich, A.D. Daniels, O. Farkas, J.B. Foresman, J.V. Ortiz, J. Cioslowski, D.J. Fox, Gaussian 09, revision A.1., Gaussian, Inc., Wallingford, CT (2009).
- [65] GaussView. Version 5, R. Dennington, T. Keith, J. Millam, Semichem Inc., Shawnee Mission, KS (2009).
- [66] Y. Zhao, D.G. Truhlar. *J. Chem. Phys.*, **125**, 194101 (2006).
- [67] J. Zheng, Y. Zhao, D.G. Truhlar. *J. Chem. Theory Comput.*, **3**, 569 (2007).
- [68] S. Torker, D. Merki, P. Chen. *J. Am. Chem. Soc.*, **130**, 4808 (2008).
- [69] Y. Zhao, D.G. Truhlar. *Theor. Chem. Acc.*, **120**, 215 (2008).
- [70] Y. Zhao, D.G. Truhlar. *Acc. Chem. Res.*, **41**, 157 (2008).
- [71] M. Korth, S. Grimme. *J. Chem. Theory Comput.*, **5**, 993 (2009).
- [72] Y. Zhao, D.G. Truhlar. *J. Chem. Theory Comput.*, **5**, 324 (2009).
- [73] A.A. Attia, A. Lupan, R. Silaghi-Dumitrescu. *RSC Adv.*, **3**, 26194 (2013).
- [74] D. Andrae, U. Häußermann, M. Dolg, H. Stoll, H. Preuß. *Theor. Chim. Acta*, **77**, 123 (1990).
- [75] M. Cossi, N. Rega, G. Scalmani, V. Barone. *J. Comput. Chem.*, **24**, 669 (2003).
- [76] H.B. Schlegel, S.S. Iyengar, X. Li, J.M. Millam, G.A. Voth, G.E. Scuseria, M.J. Frisch. *J. Chem. Phys.*, **117**, 8694 (2002).
- [77] S. De Marothy. *XYZViewer: A Software for Molecular Visualization and Simple Property Calculations*, Stockholm University, Sweden (2011).